Continental Shelf Research 29 (2009) 2110–2121

Contents lists available at ScienceDirect

Continental Shelf Research

journal homepage: www.elsevier.com/locate/csr

Dense overflow from an Arctic fjord: Mean seasonal cycle, variability and wind influence

F. Geyer [a,b,*], I. Fer [c,b], T. Eldevik [a,b]

[a] Nansen Environmental and Remote Sensing Center, Thormølensgate 47, 5006 Bergen, Norway
[b] Bjerknes Center for Climate Research, Allégaten 55, 5007 Bergen, Norway
[c] Geophysical Institute, University of Bergen, Allégaten 70, 5007 Bergen, Norway

ARTICLE INFO

Article history:
Received 26 January 2009
Received in revised form
16 July 2009
Accepted 13 August 2009
Available online 21 August 2009

Keywords:
Overflow
Arctic shelves
Barents Sea
Storfjorden

ABSTRACT

Storfjorden, an Arctic fjord in the Svalbard archipelago, is separated by a submarine sill from the adjacent shelf areas and produces one of the densest water masses in the Barents Sea. The cold and dense brine-enriched shelf water is produced through ice formation in an annually recurrent polynya in Storfjorden and overflows across the sill. We present current profiles and bottom temperature measurements from the Storfjorden sill from 2003 to 2007, which is the longest time series collected at this site, and study the interannual variability of the overflow and the influence of atmospheric forcing. The mean structure of the overflow averaged over four seasons shows that the overflow is initially strong with high volume transport, about 50 m thick and bottom-enhanced, and then gradually diminishes, becoming increasingly intermittent during the last third of the overflow season. The annual average overflow transport is about 0.03 Sv ($1\,\mathrm{Sv} \equiv 10^6\,\mathrm{m^3\,s^{-1}}$). Overflow is observed 55% of the total record length of 958 days and cross-sill flow averaged in the bottom 20 m is greater than $10\,\mathrm{cm\,s^{-1}}$ for 49% of the overflow duration. The overflow strength increases with decreasing near-bottom temperatures. The annual variability is within 0.01 Sv whereas the seasonal variability can be as large as 0.05 Sv. In spite of the relatively constant annual overflow flux, the onset of the overflow can vary by up to 50 days. Variability on the scale of 1–2 weeks is connected to wind forcing through surface Ekman transport with significant coherence between the current at the Storfjorden sill and wind measured on Hopen Island and Edgeøya. Surface Ekman transport and the ice conditions in the Barents Sea also influence the intra-seasonal development and interannual variability of the overflow.

1. Introduction

The continental shelves of the Arctic Ocean are broad and play a key role in the distribution of water properties in the Arctic basins through water mass transformations and shelf-basin interactions. Wind forcing is crucial in this complex chain of events where, for instance, summertime upwelling events can bring relatively warm and saline waters onto the shelf or wintertime prevailing offshore winds can maintain open ice-free areas (coastal polynyas). Strong heat exchange in coastal polynyas leads to ice freezing, brine-drainage and formation of dense brine-enriched shelf water (BSW), which contributes to the cold halocline in the Arctic Ocean (Aagaard et al., 1981) and significantly influences the overall heat and salt budget of the deep basins (Aagaard et al., 1985). The summertime forcing preconditions the following freezing period: upwelled saline water can lead to denser BSW or accumulated ice melt can hinder enhanced salinity regardless of significant ice production. Carmack and Chapman (2003) reported an extraordinary sensitivity of the exchange between the shelf and the deep basin to the position of summertime ice edge location. Abrupt and very effective exchange occurs when the ice edge retreats seaward off the shelf break and upwelling brings warm, salty and nutrient rich waters onto the shelf. The recent unprecedented retreat in summertime Arctic ice cover (Perovich et al., 2008) suggests that ice-free Arctic shelves can be exposed to wind forcing for longer durations. In addition to physical effects, distinct biological consequences are anticipated with enhanced Arctic spring productivity, altered marine ecosystem structure and pelagic-benthic coupling (Arrigo et al., 2008).

Storfjorden in Svalbard Archipelago (Fig. 1) is a semi-enclosed bay and provides for a relatively easily accessible and full-scale "laboratory" to study the Arctic shelf processes. The annually recurrent polynya activity in Storfjorden produces highly BSW

* Corresponding author at: Nansen Environmental and Remote Sensing Center, Thormølensgate 47, 5006 Bergen, Norway. Tel.: +47 5520 5890.
E-mail addresses: florian.geyer@nersc.no (F. Geyer), ilker.fer@gfi.uib.no (I. Fer), tor.eldevik@nersc.no (T. Eldevik).

0278-4343/$ - see front matter © 2009 Elsevier Ltd. All rights reserved.
doi:10.1016/j.csr.2009.08.003

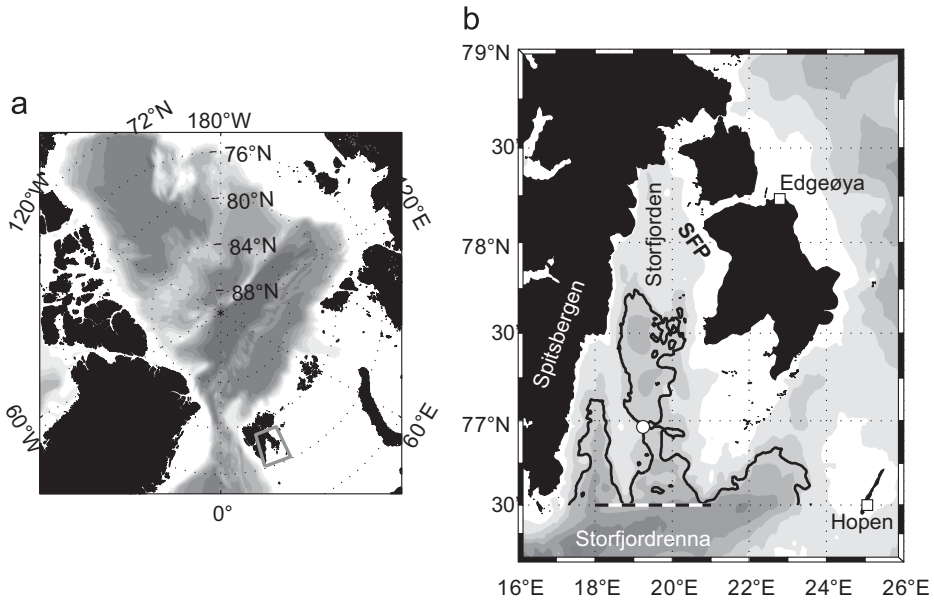

Fig. 1. (a) Overview map of the Arctic showing the enclosed region (gray) enlarged in (b). (b) Map of Storfjorden and surrounding areas showing the location of the ADCP (white circle) and the weather stations at Edgeøya and Hopen (squares). Also indicated are the most common position of the Storfjorden polynya (SFP) and the section used to calculate surface Ekman transports from ERA40 data (dashed black-and-white line). Isobaths are shaded at 500 m intervals in (a) and 50 m intervals in (b). The additional 120 m isobath in (b) is from the high-resolution bathymetry reported in Skogseth et al. (2005b), shown to identify the sill.

that fills the fjord to the sill level (115 m) and initiates a gravity driven overflow of the dense polynya-origin water (Schauer, 1995; Fer et al., 2003, 2004; Skogseth et al., 2005a). The overflow is dense enough to penetrate below the Atlantic Water in the region. Water originating from the Storfjorden polynya has been observed in the deep Fram Strait (Quadfasel et al., 1988) and may contribute to the ventilation of the Arctic Ocean (Schauer and Fahrbach, 1999). According to the estimate by Quadfasel et al. (1988), Storfjorden supplies 5–10% of the dense waters formed in the Arctic Ocean. The reader is referred to Skogseth et al. (2005b) for hydrographic characteristics and water mass transformations in Storfjorden, to Skogseth et al. (2007) for meso-scale surface circulation in Storfjorden, to Skogseth et al. (2008) for recent observations of the polynya processes and the polynya-overflow link, and to Fer and Ådlandsvik (2008) for a model description of the descent and mixing of the overflow plume.

The objective of this paper is to quantify the volume transport of the dense overflow from the sill and explain the interannual and mesoscale variability. While we focus on Storfjorden, the processes will be relevant to other polynyas on Arctic shelves. Under the DAMOCLES (Developing Arctic Modeling and Observing Capabilities for Long-term Environmental Studies) project, an acoustic Doppler current profiler (ADCP) is maintained at the sill separating Storfjorden from Storfjordrenna north of Storfjordbanken on the Barents Sea shelf (Fig. 1). Current profiles and bottom temperatures recorded by the ADCP cover four consecutive years from early winter 2003 to late spring 2007. This is the longest time series acquired at the Storfjorden sill so far. Furthermore, the ADCP offers the advantage of continuous profiling of a large fraction of the water column with high vertical resolution. The longest earlier time series (Schauer and Fahrbach, 1999) covers two non-consecutive years during the early 1990s using moored current meters measuring at two levels, supplemented by thermistor chains. Here, based on the four-year long time series, we describe the mean seasonal cycle and vertical structure of the overflow and investigate the influence of wind forcing on the preconditioning and export of water from the fjord. The data used in this study are summarized in Section 2. Following a description of the methods given in Section 3, the salient features, mean seasonal cycle, interannual, and mesoscale variability of the overflow are presented in Section 4. Subsequently the results are discussed in Section 5 followed by conclusions in Section 6.

Table 1
ADCP data recovery and periods of available meteorological data.

Location	Start	End	Instruments
Storfjorden sill	4.9.2003	19.8.2004	ADCP
	18.12.2004	11.8.2005	ADCP
	12.12.2005	9.8.2006	ADCP, Microcat
	13.8.2006	22.4.2007	ADCP
Hopen	1.1.2003	31.1.2005	met data
	25.5.2005	31.12.2007	met data
Edgeøya	19.7.2005	6.11.2007	met data[a]

[a] Wind direction data erroneous between 20.4.2006–10.10.2006 and 18.9.2007–6.11.2007.

2. Data

2.1. Current measurements

The current measurements reported here are collected by a 307 kHz Workhorse RD Instruments ADCP. The ADCP was mounted, looking upward, in a trawl-proof bottom frame. The frame was deployed at the Storfjorden sill (76°58′ N, 19°15′ E, Fig. 1) before the freezing period, and recorded through the freezing and overflow season before it was recovered in summer. Four deployments were made from 2003 to 2007 (Table 1). Recovered data cover the complete overflow seasons of 2004–2006, but coverage in 2007 lasts only until 22 April 2007 1630 UTC when the frame was hit by a trawler. During all deployments current profiles were sampled at 4-m vertical bin size, with the first bin centered at about 6 mab (meter above bottom). Profiles were averaged at 10 min intervals (33 pings per ensemble) in 2004–2006 and at 2 min intervals (13 pings per ensemble) in

2007. Processing details are reported elsewhere (Fer, 2006, 2007). In addition to profiling the horizontal and vertical velocity components, the ADCP is equipped with temperature (accuracy $\pm 0.4\,^{\circ}$C, resolution 10 mK), tilt (accuracy $\pm 0.5^{\circ}$, resolution 0.01°) and compass (accuracy $\pm 2^{\circ}$, resolution 0.01°) sensors at the instrument level (about 0.7 mab). From 2005 and on the bottom frame ballast comprises components that can affect the compass. The compass was corrected against ship-ADCP measurements available in 2005 and 2006 using an offset of $45^{\circ} \pm 20^{\circ}$ in 2005 and $0^{\circ} \pm 5^{\circ}$ in 2006 (see Fer, 2007 for details). When sampled at 4-m bins, the ADCP has a typical range of about 100 m which varies seasonally, depending on the scatterers in the water column. For the horizontal velocity, single ping standard deviation is $3\,\mathrm{cm\,s^{-1}}$.Because random error is uncorrelated from ping to ping, averaging reduces the standard deviation of the velocity error by the square root of the number of pings, yielding $0.5\,\mathrm{cm\,s^{-1}}$ ($0.8\,\mathrm{cm\,s^{-1}}$ for the 2007 deployment). In 2006, the frame was also equipped with a Sea-Bird Microcat temperature-conductivity-pressure (CTD) recording unit sampling every 10 min. The accuracy of the sensors provided by the manufacturer is $\pm 0.002\,^{\circ}$C for the temperature and $0.0003\,\mathrm{S\,m^{-1}}$ for the conductivity. The Microcat derived salinity is further corrected against CTD profiles collected prior to and after the deployment (Fer, 2007).

2.2. Meteorological data

Meteorological data from two nearby weather stations are available for the deployment period. The manned weather station on Hopen (76°30′ N, 25°4′ E) is 157 km from the Storfjorden sill and the automated weather station on Edgeøya (78°14′ N, 22°47′ E) is 164 km from the Storfjorden sill (Fig. 1). Meteorological data from Hopen are available for the deployment period with one gap in the measurements in 2005 (Table 1). The synoptic weather station at Hopen is located at the eastern side of the island. Wind from southeast and northwest, i.e. perpendicular to the orientation of the mountainous plateau inland from the station, can be biased low, influenced by the local orography. Weather data from the Edgeøya automated weather station are available only for the freezing and overflow seasons in 2006 and 2007 (Table 1). Parts of the Edgeøya wind record (between April and October 2006 and from September 2007 and on) with exceptionally steady wind direction suggest instrument malfunction and are discarded from the following analysis. Data from Edgeøya are used to verify that results obtained using data from Hopen are applicable to Storfjorden.

3. Measuring the overflow

In order to delineate the dense overflow across the Storfjorden sill and estimate overflow volume transport, we use the following definition and criteria of the overflow in the present data set. In the calculations we use hourly averaged, 40-h low-passed data in order to exclude tidal motions and high-frequency variability. The sill is aligned zonally, less than 2° counterclockwise from east. This is less than the compass accuracy and we refer to the north component v of the horizontal velocity as the cross-sill component with negative values directed out of the fjord. Additionally, we define the outflow speed, u_{out}, as the modulus of the velocity directed to within $90-270^{\circ}$ T. This range of direction is chosen because the overflow has a significant along-sill component (Section 4.2). Transport estimates derived using the cross-sill component alone are typically 30% smaller. Overflow is assumed to occur when two conditions are met simultaneously: (i) the bottom temperature is below the upper limit for BSW ($T_{BSW} < -1.5\,^{\circ}$C), which forms the source of the Storfjorden overflow, and (ii) the outflow speed u_{out} averaged in the bottom 20 m (deepest 5 bins) exceeds $2\,\mathrm{cm\,s^{-1}}$, thus ensuring measurable overflow. This sampling identifies the onset and termination of the overflow season as the first and the last instances satisfying these conditions for each deployment, as well as the times of overflow throughout an overflow season. We define the overflow season length as the time between the onset and termination of the overflow season. We define the overflow duration as sum of the time of overflow occurrences. Because the overflow can be intermittent, the overflow season length and the overflow duration can be different. We define the intermittency, I, as the percent of the overflow season with no overflow occurrence.

The overflow volume transport is $Q = \langle u_{\mathrm{out}} \rangle hB$, where u_{out} is the outflow speed (defined above), B is the width, and angle brackets denote averaging over the overflow thickness, h. We assume a constant overflow width of $B = 15$ km following an estimate deducted from mooring observations by Schauer (1995) and Schauer and Fahrbach (1999), and consistent with the width used in the transport estimates by Schauer (1995). The assumption of a constant plume width is a major simplification and further discussed in Section 4.3. At each profile which satisfies the overflow criteria, we estimate the plume thickness, as the height where the outflow reaches a velocity threshold. The threshold is chosen in such a way that it separates the bottom-enhanced flow from a background flow. This serves as the best identification of the dense overflow in the absence of temperature and salinity profiles. In order to define the threshold, which varies with the strength of the overflow, we sample the velocity profiles in groups according to the mean outflow velocity in the bottom 20 mab. Ensembles falling into $5\,\mathrm{cm\,s^{-1}}$ increment bins are normalized by the maximum outflow within 20 mab and then averaged (Fig. 2).

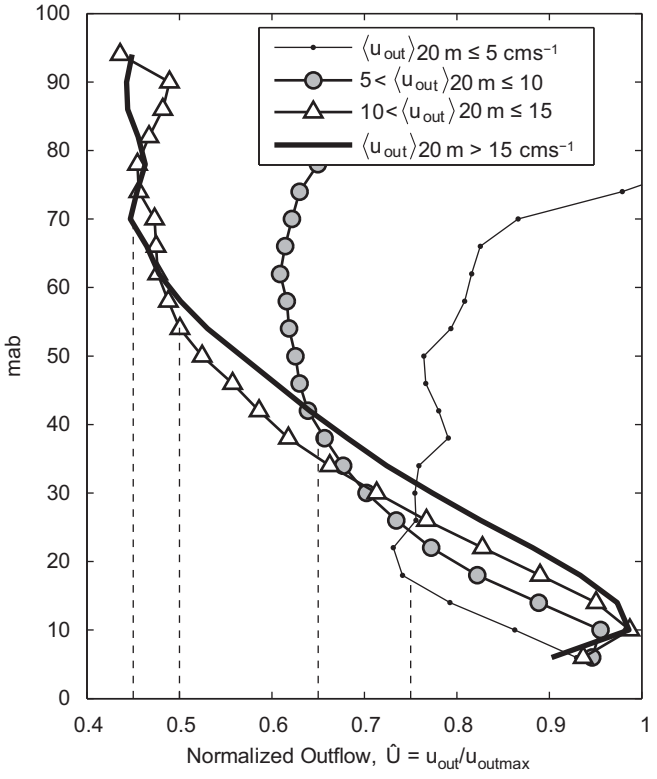

Fig. 2. Profiles of outflow velocity normalized by the maximum outflow in the bottom 20 mab. Ensembles are averaged in $5\,\mathrm{cm\,s^{-1}}$ bins of the average outflow in the bottom 20 mab. Vertical dashed lines mark the thresholds that are used to determine the plume thickness.

Normalized profiles of these groups are used to determine a non-dimensional velocity threshold that identifies the overflow height as the height where the bottom-enhanced flow vanishes (Fig. 2). The identified non-dimensional velocity thresholds are then applied to each instantaneous velocity profile to construct overflow height time series. At instances when the threshold is not met, the height of the velocity minimum for that profile is used.

4. Results

4.1. Overflow characteristics

Time series of current data from the four deployments (Table 1) are merged and presented in Fig. 3. Three complete overflow seasons from 2004 to 2006 and part of the overflow season in 2007 are covered. Temperatures close to the freezing point can be seen to coincide with a strong and persistent cross-sill flow out of the fjord. At higher temperatures the cross-sill flow is more intermittent. During the periods of strong outflows, the flow often extends more than 60 m from the bottom. In large parts of the record, the currents at the Storfjorden sill vary little with depth for the recorded depth range (Fig. 3). For the 40-h low-passed cross-sill current within the range of the ADCP the variance of the depth-averaged current explains 78% of the total variance. The cross-sill component of the current (north–south) is generally stronger than the along-sill component (east–west).

The connection between the bottom temperature and the cross-sill flow is clearly identified when the profiles and the bottom temperature are ensemble averaged according to the strength of the bottom current (Fig. 4). On average the coldest cross-sill flow directed out of fjord is strongest and enhanced towards the bottom. Outflow at intermediate temperatures is weaker and nearly uniform with depth. All significant inflow is associated with above zero temperatures. The current profiles show that while the flow is bottom-enhanced, the current direction stays consistently in or out of the fjord up to more than 80 m above the bottom. The most frequently observed bottom speeds range from 0 to 15 cm s^{-1}, directed out of the fjord. Velocity profiles with strong flow display sign of a frictional bottom boundary layer.

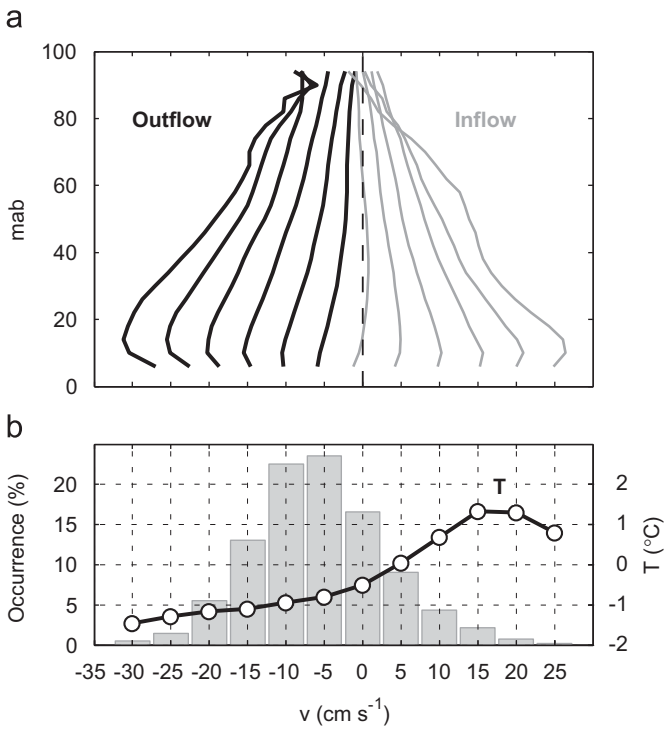

Fig. 4. (a) Average current profiles for the north (cross-sill) component of the velocity grouped according to the 20 mab averaged bottom current in 5 cm s^{-1} increments. Black (gray) traces mark outflow (inflow). (b) Histogram of northward bottom current (vertical bars) and the corresponding average bottom temperature for each velocity bin (circles).

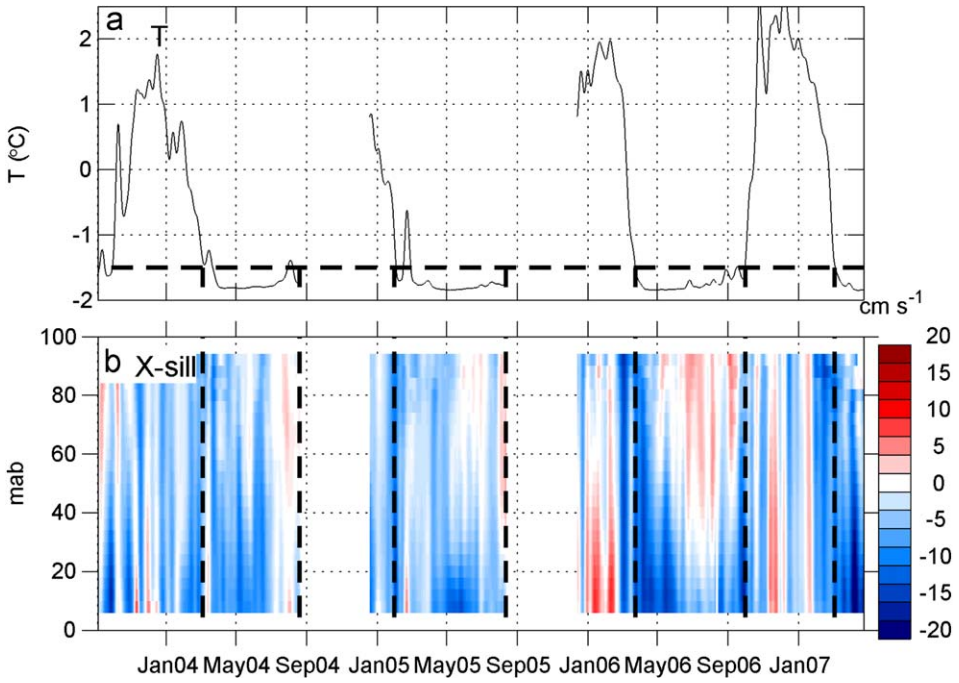

Fig. 3. Time series of (a) bottom temperature and (b) cross-sill component of the velocity (negative values out of the fjord) for the period covering all four deployments. 15-day low-passed hourly data are shown. Vertical dashed lines mark the times of overflow onset and end. Horizontal dashed line in (a) is the upper limit for BSW temperature equal to −1.5 °C.

4.2. Mean overflow cycle

Using the overflow definition of Section 3, the present data set enables us, for the first time, to present the mean structure of the overflow (Fig. 5). The time (days following the onset of the overflow) of each year is normalized by the overflow season length. Year 2007 covers less than half of a typical overflow season, and it is assigned a season length equal to the mean length of 2004–2006. The inferred season length and overflow duration are summarized in Table 2. The mean overflow cycle is then obtained as the ensemble average of the four seasons in 0.05 unit normalized time bins. The overflow is, on average, between 20 and 50 m thick and clearly bottom-enhanced (Fig. 5d). The mean overflow flux during the overflow season is 0.05 Sv (Fig. 5e). While the across-sill velocity component is dominating in the beginning of the overflow season, the along-sill velocity component becomes comparable around the middle of the overflow season (Fig. 5a, b). In the beginning and during the last third of the overflow season bottom temperatures are higher compared to the rest of the season, and the overflow is more intermittent (Fig. 5c). Both the plume thickness and the overflow flux are largest early in the overflow season and then decline gradually. The high fluxes early in the overflow season occur in spite of the increased intermittency. Initially the overflow is almost uniform with height, with out-fjord velocities above the plume comparable to those near the bottom (Fig. 5d). As the bottom temperature approaches freezing the velocity profile increases towards the bottom.

4.3. Overflow volume transport

Transport estimates are made every hour using 40-h low-passed outflow velocities as described in Section 3. The resulting 14-day averages and standard deviations are shown in Fig. 6, together with the inferred plume height and the mean outflow speed. An overview of annual overflow fluxes is given in Table 3. The average transports in 2004 and 2005 are identical, and are comparable to that in 2006. The relatively large 0.11 Sv estimate for 2007 does not account for the later part of the overflow season, when transport typically declines (Fig. 5e). When the commonly sampled time period is considered, average transport between 1 January and 22 April is largest in 2007. The interannual variability is discussed in the next section.

Possibly the largest uncertainty in the volume transport estimate is the constant 15 km width assumption. Hydrographic coverage of the sill during the most active period of the overflow is extremely scarce: There exists one hydrographic profile directly at the sill and one nearby in April 2001 taken by a helicopter survey (Fer et al., 2003). There also exist a few profiles at the easternmost edge of the sill taken during an ice-breaker based survey in April 2006 (Skogseth et al., 2008). Fer and Ådlandsvik (2008) concluded from a regional model study that the flow at the sill is geostrophic and the tilt of the interface can be inferred from the density anomaly of the plume. This practical result that can give an estimate of the width B, however, cannot be applied here directly due to the scarcity of density profiles. Rossby radius

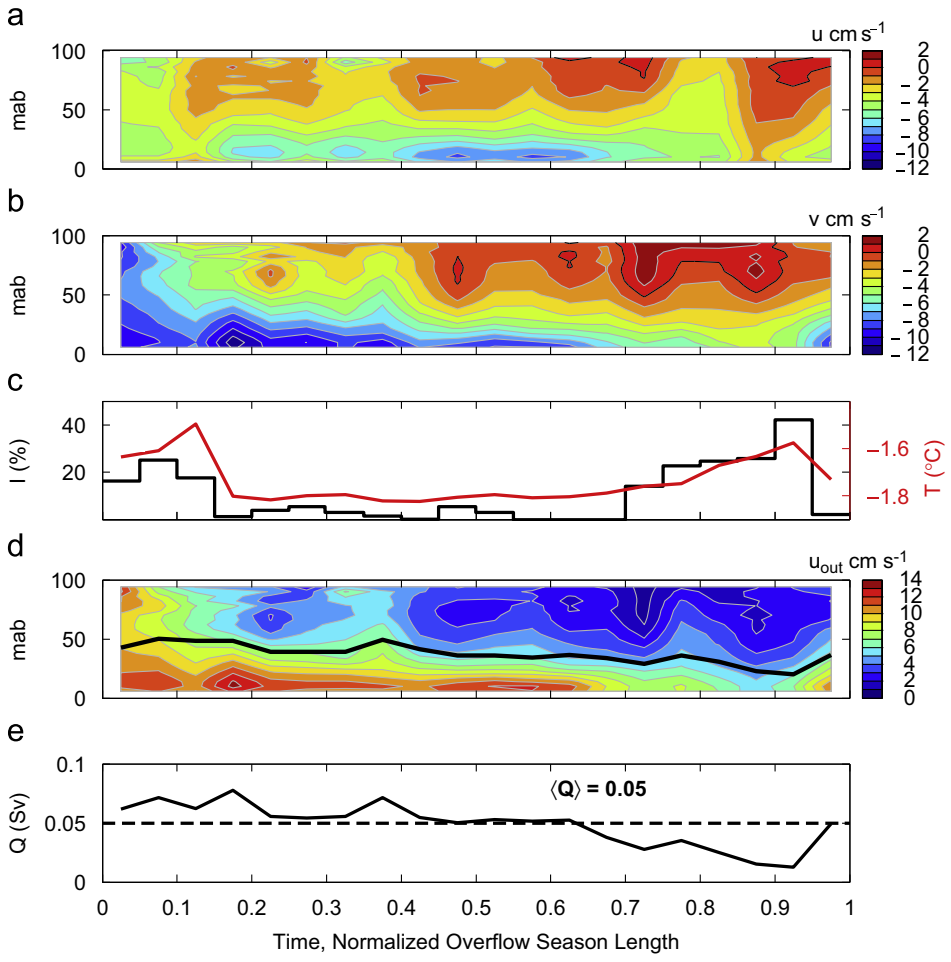

Fig. 5. Mean seasonal cycle of the Storfjorden overflow shown as a function of time normalized by overflow season length. (a) Velocity towards east (along-sill), zero isotach in black, (b) velocity towards north (cross-sill), zero isotach in black, (c) bottom temperature (red) and intermittency (black), (d) outflow velocity u_{out} and (black) overflow height inferred from velocity profiles, and (e) overflow volume flux. Dashed horizon shows the seasonal average of 0.05 Sv.

Table 2
Storfjorden overflow overview 2004–2007.

Start	End	Overflow season length (% of year)	Overflow duration (% of year)
4.3.2004	19.8.2004[a]	46	36
30.1.2005	11.8.2005[a]	53	48
23.3.2006	30.9.2006	52	47
3.3.2007	22.4.2007[a]	–[b]	–[b]

[a] End of overflow season due to end of data record.
[b] Only part of the overflow season is observed. The observed part of the season length and the overflow duration would correspond to 14% of year.

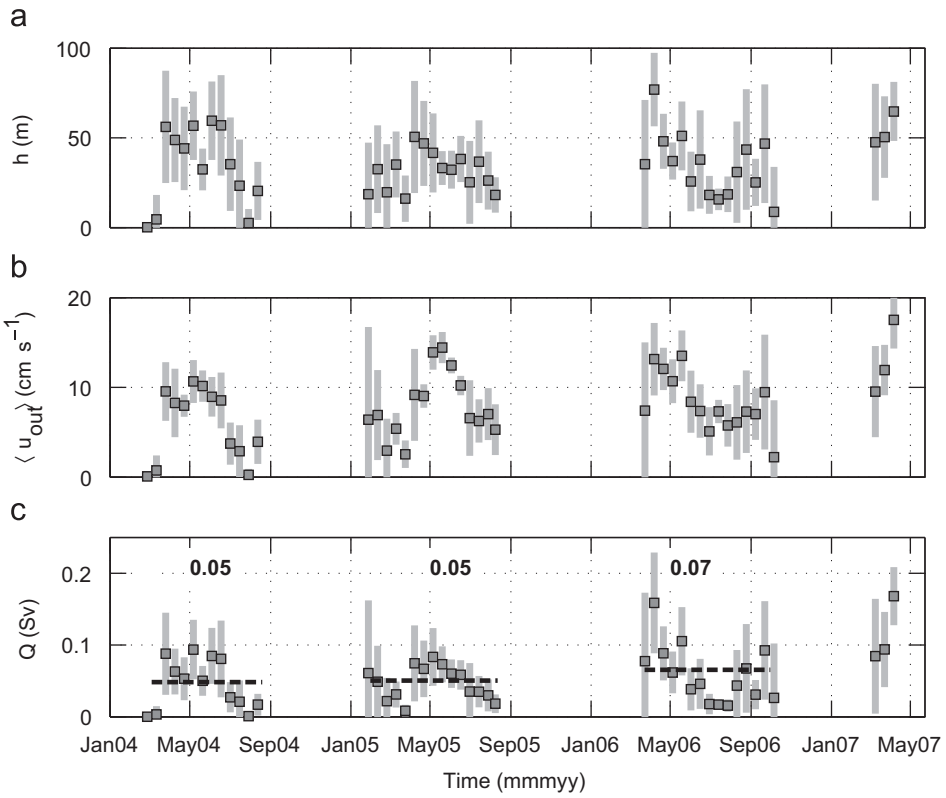

Fig. 6. 14-day mean (square) and standard deviation (vertical bars) for (a) overflow plume thickness h, (b) outflow speed averaged over the extend of h, and (c) volume transport Q assuming a plume width of 15 km. Also shown in (c) are the mean values of Q, in Sv, for each overflow season. The mean transport for the observed part of the overflow season in 2007 is 0.11 Sv.

Table 3
Comparison of annual averaged overflow fluxes from ADCP data to estimates from earlier measurements.

Data	Location	Year	Flux (Sv)
RCM, T-chain	30 km S of sill	1992	0.05[a]
LADCP	65 km SW of sill	2001	0.06[b]
Polynya model	Polynya	1998–2002	0.03–0.04[c]
ADCP	Sill	2004	0.022
ADCP	Sill	2005	0.027
ADCP	Sill	2006	0.034
ADCP	Sill	2007	–[d]

[a] Schauer (1995).
[b] Fer et al. (2003), snapshot.
[c] Skogseth et al. (2005a), BSW production.
[d] Only part of the overflow season is covered in 2007. The observed part of the overflow would correspond to a yearly average transport of 0.015 Sv. When averaged until 22 April, overflow flux in 2007 is 2.3 times that in 2004, and 1.4 times that in 2005 and 2006.

estimates from the scarce hydrological data are on the order of 1–2 km. Given the model results by Fer and Ådlandsvik (2008) that the width of the plume corresponds to 8–20 times the local Rossby radius our estimate of 15 km width is reasonable. The ice-breaker stations show that the BSW plume at the sill can reach a width of up to 40 km. Nonetheless, the width of 15 km is likely representative of the overflow season average, because relatively wide overflow early in the season (e.g., April observations of Skogseth et al., 2008) is expected to narrow as the overflow weakens throughout the season. The uncertainties involved in the transport calculation, however, make the obtained flux estimate uncertain by 50%.

4.4. Interannual variability

There is substantial variability from the mean overflow cycle described above, both with respect to the onset of the overflow

season and the intra-seasonal development. The overflow starts 30–50 days earlier in 2005 than in the other years. The transition period from relatively high bottom temperatures to near freezing point is shorter in 2006 and 2007 compared to 2004 and 2005. Interannual variability can also be seen in the development of the cross-sill flow during the overflow season, e.g., varying degree of depth dependency or the period of strongest cross-sill currents in the season (Fig. 3).

The sequence of monthly mean current profiles is qualitatively similar for 2003–2007, but within a substantial range of variability (Fig. 7). In January and February 2006, the bottom flow, on average, is directed into the fjord, in contrast to net outflow throughout the whole water column in other years. April and March profiles show the strongest overflow in 2006 and 2007, with velocities approximately twice those of the preceding years. The overflow persists throughout the water column in June 2004, while the other years show weaker overflow limited to the bottom 50–70 m. Interannual variations for a particular month can be comparable to the variability within the overflow season.

Progressive vector diagrams for the commonly sampled time period (Fig. 8), however, show the overall similarity from year to year: The northward cumulative displacement of the overflow is similar, the flow is generally directed south to southwest being strongest near the bottom. The differences in overall current direction might be due to uncertainties in the compass corrections (Fer, 2007).

The overflow season length and the duration of overflow are about 10% shorter in 2004 than in 2005 and 2006 (Table 2). The overflow in 2005 starts relatively early. For the years with coverage of the complete overflow season (2004–2006), overflow in 2006 was strongest on average. For the part of the overflow season covered in all years, the average volume transport in 2007 is stronger than the preceding years, comparable to the strong initial overflow in 2006.

4.5. Mesoscale variability

Spectra (Gonella, 1972) of the rotary velocity components of current at the Storfjorden sill and wind at the weather stations at Hopen and Edgeøya show increased variance for periods longer than 2 days, but the spectra are essentially featureless (not shown). The reconstructed current variations for the longest periods (1.6–16 days) are nearly rectilinear and mostly oriented north–south. The coherency-squared and phase are derived from the rotary cross-spectral analysis of vertically averaged velocity and the wind vector. The results for the rotary components with the same sense of rotation (inner rotary spectrum, Livingstone and Royer, 1980) reveal significant coherence for periods longer than 4 days for both rotary components (Fig. 9). The similar coherence for the clockwise and counterclockwise components suggests a connection between the rectilinear variations of current and wind. The analysis is repeated using the shear between the velocity in the deepest bin (6 mab) and that at mid-depth (54 mab) to approximate the baroclinic current component. Results for the shear are similar with coherence significant at 99% confidence level extending to periods longer than 2 days (Fig. 10).

The connection between the cross-sill flow and wind, and the influence of wind direction on the cross-sill flow variability are explored using lagged cross-correlation between the cross-sill flow at the sill and wind data from Hopen and Edgeøya. Velocity is averaged in 6 h intervals, consistent with the wind data. Both time series are 30-day high-passed and linearly detrended prior to cross-correlation calculations. Wind directions are tested in steps

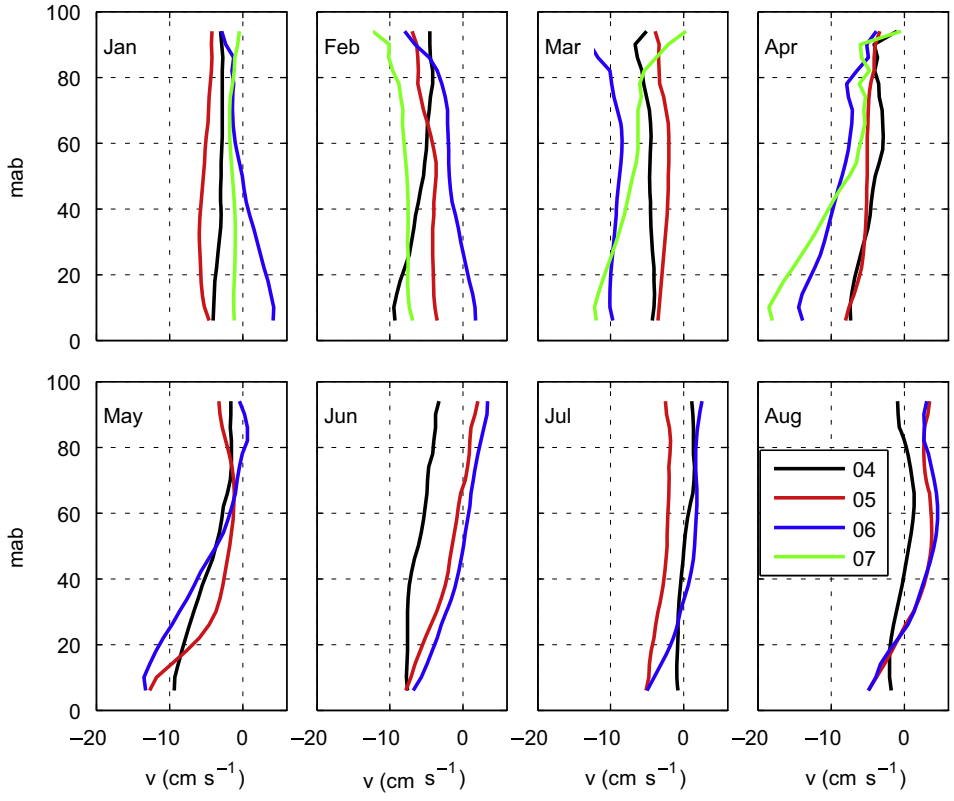

Fig. 7. Monthly mean current profiles for the north component of the velocity shown for year 2004 (black), 2005 (red), 2006 (blue) and 2007 (green). Negative values indicate approximately cross-sill flow directed out of the fjord.

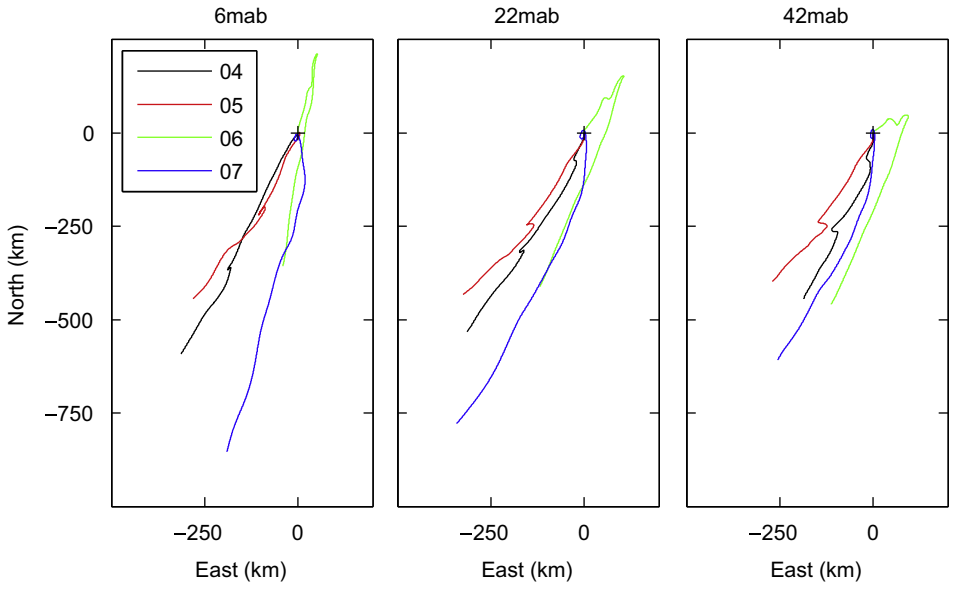

Fig. 8. Progressive vector diagrams for the period 1 January to 22 April in 2004 (black), 2005 (red), 2006 (blue), and 2007 (green) derived from the measurements 6, 22 and 42 meter above bottom (mab). 15-day low-passed data are shown.

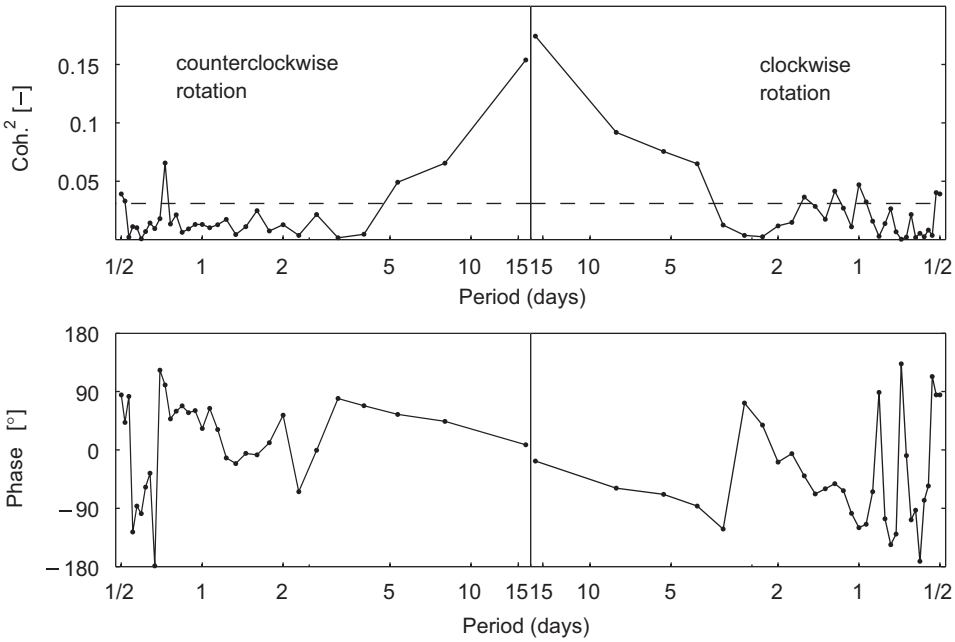

Fig. 9. Coherency-squared (upper panel) and phase (lower panel) between the counterclockwise and clockwise rotating depth-averaged current velocity at the sill and wind velocity measured at 10 m height at Hopen. Dashed line in the upper panel denotes 99% significance against white noise. Spectra are calculated using 111 64-point Hanning windows with 50% overlap (296 degrees of freedom).

of 5° to determine the optimal wind direction giving the highest correlation with the cross-sill current. Analysis reveals the correlation between the wind from northerly and north-easterly directions and both the depth-averaged and the bottom flow out the fjord (Fig. 11). Direct comparison of wind and cross-sill currents reveals that the covariation is robust, not limited to a small number of peaks but is persistent throughout the complete record.

5. Discussion

The mean seasonal cycle shows an overflow period of 180 days duration. The overflow is typically strong with high volume transports from the beginning of the overflow season despite the initial intermittency of the overflow (Fig. 5c, e). The overflow then gradually declines, becoming again intermittent during the last third of the overflow season. The average current profile is strongest and bottom-enhanced, associated with the lowest bottom temperature, close to the freezing point (Fig. 4). Weak, uniform southward flow with relatively higher bottom temperatures is likely linked to the cyclonic background circulation in Skogseth et al. (2007). Inflow of warmer water is connected to events of strong inflow of Atlantic Water into the fjord which would normally be concentrated on the eastern side of the fjord (Skogseth et al., 2005b). While flow across the sill is bottom enhanced the current direction is, on average, consistent up to

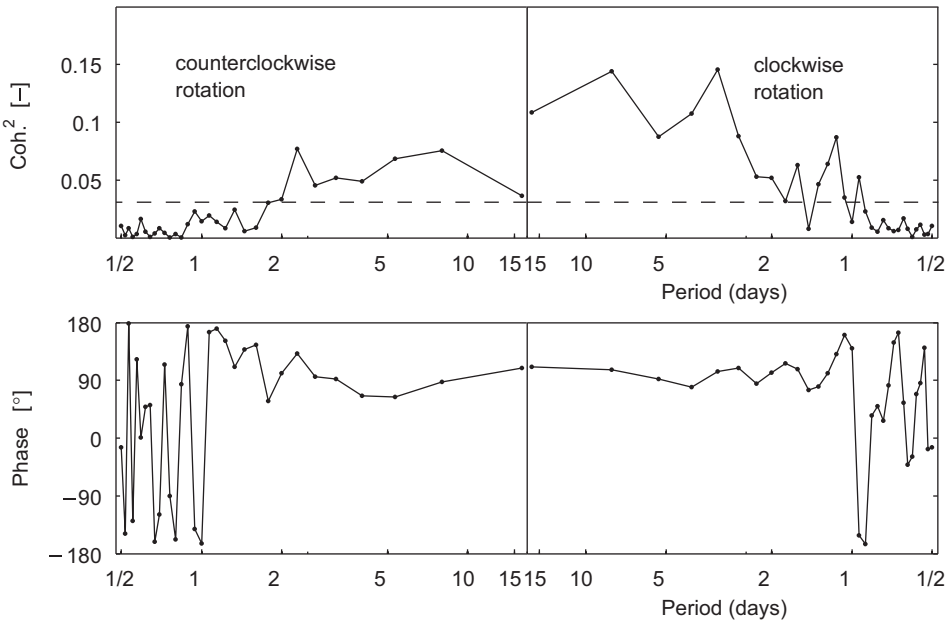

Fig. 10. Same as Fig. 9, but shown for Hopen wind and the shear between 6 and 54 mab.

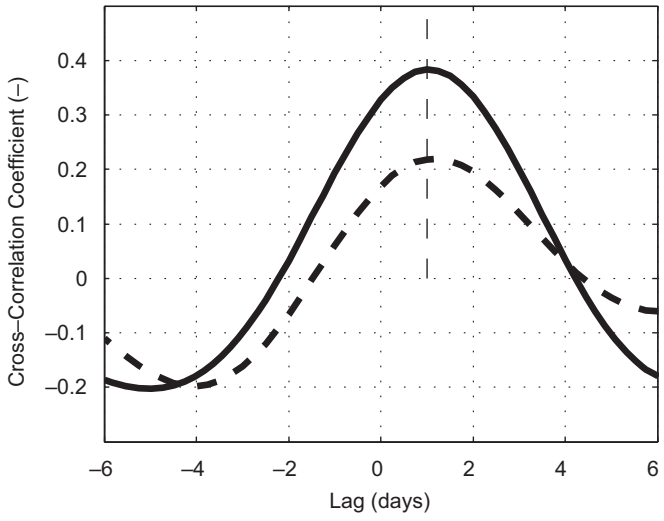

Fig. 11. Lagged cross-correlation coefficient between 7-day low-passed most favorable directed wind component and cross sill current, (solid line) wind from 45° T and depth-averaged current, (dashed line) wind from 35° T and shear between 6 and 54 mab. Wind speed is sampled at 10 m height every 6 h. Currents are 6-hourly averaged to be consistent with the wind data. Vertical dashed lines mark the lag of the highest correlation at 1 day with wind leading the current at the sill.

more than 80 m above the bottom (Fig. 4). Accordingly, the depth-averaged current contribution to the total variance is dominant.

The seasonally averaged overflow volume transport estimates at the Storfjorden sill from four years of ADCP data are roughly constant (with the caveat of assuming a constant overflow width), but the intra-seasonal pattern and the onset date of the overflow show considerable variation (Fig. 6). In 2007 the average flux was larger than in other years, but this estimate is biased high because less than half the overflow season in 2007 was sampled. Comparably long periods of increased overflow flux existed in other years, e.g. in 2006. From observations of an high-salinity front after a supercooling event in the Storfjorden polynya and observations of the corresponding salinity front recorded by the Microcat at the sill in April 2006, Skogseth et al. (2008) suggest a travel time for a high salinity signal from the polynya to the sill of 12–18 days. If the strongest overflow is linked to the supply of BSW from the polynya in response to strong offshore wind events, a coherency at these time scales is anticipated. Consistently, the coherency spectrum for the clockwise rotary shear and wind (Fig. 10) shows significant coherence at weekly time scales with 90° phase difference.

Yearly averaged overflow volume transports inferred here can be compared to earlier relevant estimates (Table 3). To date, there is no observationally based study that reports the overflow volume transport at the sill. Of the relevant previous work, Schauer (1995) gives a coarse estimate of the volume flux 30 km downstream of the sill using year-long near-bottom current measurements. Farther downstream, from a 6-day survey, Fer et al. (2003) give a snapshot estimate. On the upstream, in the polynya, BSW production rate is estimated by Skogseth et al. (2005a). The overflow fluxes at the sill in 2004–2005 are slightly lower than, but that in 2007 is within the range of the BSW production rates in the Storfjorden polynya between 1998 and 2002 (Skogseth et al., 2005a). The interannual variability of the annual volume flux at the sill (2004–2006) is comparable to that inferred from the polynya model (1998–2002), suggesting that Storfjorden consistently exports about 0.03 Sv dense water, annually. There is a clear difference between the volume transport estimates downstream of the sill and those at the sill. Keeping in mind the interannual variability and measurement uncertainty, a fraction of the surplus volume flux 30–60 km downstream of the sill can be attributed to the entrainment of ambient water, increasing the volume transport significantly (Fer and Ådlandsvik, 2008). Furthermore Schauer (1995) had assumed a constant overflow height of 30 m and used the speed measured near the bottom which could be an overestimate because the strong overflow events are bottom-enhanced (Fig. 4). In summary we find our transport estimates consistent with, but on a firmer observational footing, than those of previous studies.

Using our volume transport estimates and the Storfjorden hypsometry derived from high-resolution bathymetry published by Skogseth et al. (2005b) it is possible to estimate the winter residence time of dense water in Storfjorden. The dense water fills Storfjorden up to the sill level before it starts flowing over the sill. The fjord volume below the sill level is 54 km^3. With the

estimated mean overflow volume transport of 0.05 Sv, this corresponds to a winter residence time below the sill level of 12.5 days. Skogseth et al. (2008) report a filling time of 14 days for Storfjorden below the sill level. During summer time the residence time in Storfjorden is dominated by the coastal current which flows in a cyclonic sense along the coast of Storfjorden. No direct current measurements of the coastal current exist and available transport estimates are for the baroclinic transport inferred from hydrography. From four years of CTD observation Skogseth et al. (2005b) report 0.04, 0.04, 0.11 and 0.04 Sv for the years 1999–2002 (Fig. 12). The range of 0.04–0.11 Sv for the coastal current and the complete Storfjorden volume of 850 km^3 give a residence time of 90–246 days. The volume of the upper 50 m, a depth chosen to be representative of the shallow coastal areas and the polynya, is 488 km^3 and would have a residence time of 51–141 days before the freezing season allowing for sufficient exposure for preconditioning and response to wind forcing. For a more detailed discussion on the flushing of the Storfjorden polynya, the ventilation of the basin and the corresponding timescales, see Skogseth et al. (2008).

Skogseth et al. (2008) state that brine production was poor in 2004 and moderate in 2006 compared to previous years. The low salinity of the polynya water in 2004, despite significant ice production (second largest since winter 1998), is a result of dense ice conditions in the region in the previous winter. During summer, a relatively thick melt water surface layer forms. In the following freezing period, although the ice production can be substantial, polynya-derived water cannot reach high salinity (Skogseth et al., 2008). A drawback in our data set is the lack of near-bottom salinity measurements at the sill (only available in 2006). Our methods will detect overflow as long as the near-bottom temperature is low and there is sufficient density difference across the sill which leads to a pressure gradient supporting outflow. Nonetheless, consistent with Skogseth et al. (2008), the annual average volume flux in 2004 is the minimum of our 2004–2006 observations, suggesting weak overflow. However, a later onset of the overflow in 2006 is observed compared to 2004 (Section 4) despite the better preconditioning in 2006.

The variability of the current on a time scale of 1–2 weeks can, for large parts of the record, be attributed to wind forcing. This is evidenced by the significant rotary coherence between current and wind (Fig. 9) and the covariation between southward flow across the Storfjorden sill and wind from northeasterly directions (Fig. 11). Wind anomalies of about 5 m s^{-1} correspond to cross-sill current anomalies of about 5 cm s^{-1}. The suggested mechanism is the surface Ekman transport into the fjord caused by the northeasterly winds. This is balanced by a flow at depth at the Storfjorden sill, if the exchange through the narrow straits close to the northern end of Storfjorden and across the ridge which forms the south-western boundary of the Storfjorden basin (Fig. 1) is neglected. The Ekman flux into the fjord is $F_E = \tau l/\rho_W f$, with the along-wind length of the southern fjord opening l, density of sea water $\rho_W = 1027\,kg\,m^{-3}$ and the Coriolis parameter $f = 1.42 \times 10^{-4}\,s^{-1}$. Wind stress $\tau = c_D \rho_A U_{10}^2$ is calculated from the wind speed at 10 m height U_{10} using a drag coefficient $c_D = 2.7 \times 10^{-3}$, a typical value for the marginal ice zone (Guest et al., 1995), and the density of air $\rho_A = 1.25\,kg\,m^{-3}$. The Ekman flux into the fjord is calculated from ERA Interim reanalysis wind

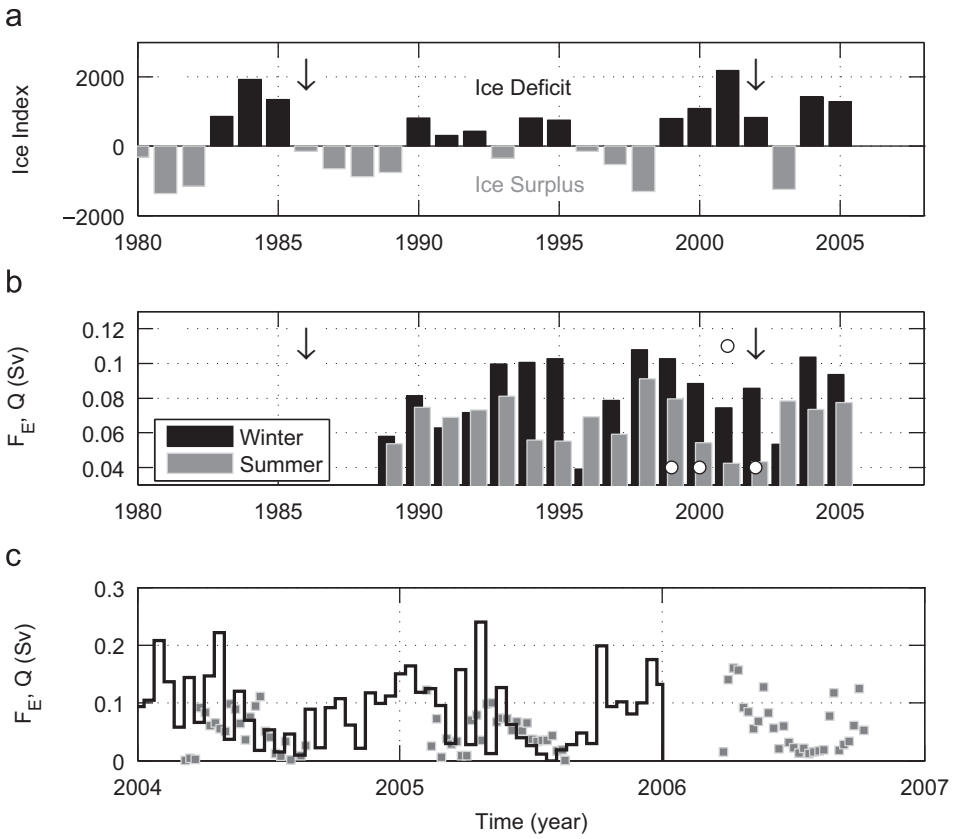

Fig. 12. Time series of (a) Barents Sea ice index (b) northward surface Ekman flux F_E, averaged for winter (first 6 months, black) and summer (last six months, gray) (c) 2-weekly northward Ekman flux F_E (black line) compared with the overflow volume flux Q at the sill (squares). The arrows in (a) mark years 1986 and 2002 when Storfjorden-origin water was observed in deep Fram Strait. The white circles denote the estimates of the baroclinic component in the coastal current in Storfjorden (Skogseth et al., 2005b). The Barents Sea ice index is an indicator for the areal extent of sea ice, negative values indicate severe ice conditions whereas positive values indicate less ice than average (Ådlandsvik and Loeng, 1991).

data (Uppala et al., 2008) using a section from 18°E to 21°E at 76.5°N, across a fjord opening of $l = 117$ km. The easterly wind component is integrated separately to obtain the in-fjord (northward) F_E.

Comparison with the overflow measurements at the Storfjorden sill shows that the surface Ekman transport and the overflow are connected not only at the time-scale of 1–2 weeks but also on longer time scales. The northward Ekman flux scales well with the intra-seasonal development of the overflow volume transport (Fig. 12c). Somewhat higher Ekman fluxes than overflow volume transports are expected, as some of the surface transport can escape through the shallow straits between Spitsbergen and the adjacent islands in the northern part of the fjord.

On an interannual time-scale both the surface Ekman transport and the ice conditions in the Barents Sea influence the strength and salinity of the Storfjorden overflow. While it is not known how much the volume transport varies during the years prior to our observations, the brine production in the Storfjorden and hence the salinity of the Storfjorden overflow are variable (Skogseth et al., 2005a). The Barents Sea ice index is an indicator for the areal extent of sea ice, calculated as the ice-free area north of 79°N in summer and as the ice-covered area south of 76°N in winter (Ådlandsvik and Loeng, 1991). Severe ice conditions appear as negative anomalies. After 2005, the index is no more applicable due to the strong recent retreat of the ice cover in the Barents Sea (Randi Ingvaldsen, 2009, personal communication). So far, two incidents have been reported when polynya water from Storfjorden has reached the Fram Strait in 1986 (Quadfasel et al., 1988) and 2002 (Rudels et al., 2005). Both years are marked by arrows in Fig. 12. The Storfjorden overflow signature in the Fram Strait was not systematically surveyed and, due to lack of observations, we cannot exclude the possibility of deep reaching overflow in other years. The Barents sea ice index documents an ice deficit in the respective year before and consistently several years back (Fig. 12a). This relates to a favorable preconditioning for the production of brine-enriched shelf water as there will be less surface melt water present in the region around Storfjorden. Furthermore the northward integrated Ekman flux influences the overflow activity. For example the weak summer Ekman flux into the fjord in 2001 (Fig. 12b) will transport less melt water from the surroundings into Storfjorden, which again preconditions for the production of relatively saline BSW. In the winter of 2002, there is a significant inflowing Ekman flux, which by continuity can boost the outflow and help explain the strong overflow observed in that year. An example of a relatively weak overflow year is 2004. The preceding summer in 2003, following a winter with ice surplus (Fig. 12a) will lead to increased surface melt water. Summer Ekman transport into the fjord in 2003 is also significant (Fig. 12b), accumulating surface melt water towards the polynya region. These factors will lead to preconditioning of the fjord unfavorable for the production of BSW.

6. Conclusions

The dense overflow season at the Storfjorden sill lasts about 180 days on average. The annual mean overflow volume transport is 0.026 Sv. The overflow starts up strongly with high volume transports early in the overflow season and then gradually diminishes, becoming increasingly intermittent during the last third of the overflow season. The comparison of four consecutive overflow seasons shows annual variability within 0.01 Sv whereas the seasonal variability can be as large as 0.05 Sv. The relatively small interannual variability is consistent with nearly constant yearly production rates of brine-enriched shelf water (BSW) at the Storfjorden polynya reported by Skogseth et al. (2005a). There are, however, considerable variations in the onset date and the intra-seasonal distribution of the overflow flux. These variations are especially prominent when comparing specific months of different years. Variability of the cross-sill flow on the shorter scale of 1–2 weeks is strongly connected to wind forcing throughout, as evidenced by the significant rotary coherence of current and wind. The suggested physical mechanism is surface Ekman transport into and out of the fjord caused by, respectively, northeasterly and southwesterly winds. On an interannual time-scale the surface Ekman transport and the Barents Sea ice index can be used as indicators on the strength of the Storfjorden overflow. Low summer Ekman transports and an ice deficit in the Barents Sea in the preceding year relate to a favorable preconditioning for BSW production in Storfjorden and thus to a more saline and deep-reaching overflow.

Acknowledgments

This work is partly funded by the Research Council of Norway, through Bipolar Atlantic Thermohaline Circulation (BIAC) project. The Damocles project is financed by the European Union in the 6th Framework Programme for Research and Development. This is publication no. A-246 from the Bjerknes Center of Climate Research.

References

Aagaard, K., Coachman, L.K., Carmack, E., 1981. On the halocline of the Arctic Ocean. Deep-Sea Res. 28A, 529–545.
Aagaard, K., Swift, J.H., Carmack, E., 1985. Thermohaline circulation in the Arctic Mediterranean Seas. J. Geophys. Res. 90, 4833–4846.
Ådlandsvik, B., Loeng, H., 1991. A study of the climatic system in the Barents Sea by a wind-driven model. Polar Res. 10, 45–49.
Arrigo, K.R., van Dijken, G., Pabi, S., 2008. Impact of a shrinking Arctic ice cover on marine primary production. Geophys. Res. Lett. 35, L19603 10.1029/2008GL035028.
Carmack, E., Chapman, D.C., 2003. Wind-driven shelf/basin exchange on an Arctic shelf: the joint roles of ice cover extent and shelf-break bathymetry. Geophys. Res. Lett. 30, 1778 10.1029/2003GL017526.
Fer, I., Skogseth, R., Haugan, P.M., Jaccard, P., 2003. Observations of the Storfjorden outflow. Deep-Sea Res. Part I 50, 1283–1303.
Fer, I., Skogseth, R., Haugan, P.M., 2004. Mixing of the Storfjorden overflow (Svalbard Archipelago) inferred from density overturns. J. Geophys. Res. 109, C01005 10.1029/2003JC001968.
Fer, I., 2006. Current measurements at the Storfjorden sill, September 2003 to August 2004. Reports in Meteorology and Oceanography, Geophysical Institute, University of Bergen. Report No. 1-2006, 41pp., ISBN 82-8116-007-1.
Fer, I., 2007. Current measurements at the Storfjorden sill, 2004–2006. Reports in Meteorology and Oceanography, Geophysical Institute, University of Bergen. Report No. 1-2007, 26pp., ISBN 82-8116-012-8.
Fer, I., Ådlandsvik, B., 2008. Descent and mixing of the overflow plume from Storfjord in Svalbard: an idealized numerical model study. Ocean Sci. 4, 115–132.
Gonella, J., 1972. A rotary-component method for analysing meteorological and oceanographic vector time series. Deep-Sea Res. 19, 833–846.
Guest, P.S., Glendening, J.W., Davidson, K.L., 1995. An observational and numerical study of wind stress variations within marginal ice zones. J. Geophys. Res. 100, 10887–10904.
Livingstone, D., Royer, T.C., 1980. Eddy propagation determined from rotary spectra. Deep-Sea Res. Part A 27, 823–835.
Perovich, D.K., Richter-Menge, J.A., Jones, K.F., Light, B., 2008. Sunlight, water, and ice: extreme Arctic sea ice melt during the summer of 2007. Geophys. Res. Lett. 35, L11501 10.1029/2008gl034007.
Quadfasel, D., Rudels, B., Kurz, K., 1988. Outflow of dense water from a Svalbard fjord into the Fram Strait. Deep-Sea Res. 35, 1143–1150.
Rudels, B., Björk, G., Nilsson, J., Lake, I., Nohr, C., 2005. The interactions between waters from the Arctic Ocean and the Nordic Seas north of Fram Strait and along the East Greenland Current: results from the Arctic Ocean-02 Oden Expedition. J. Mar. Syst. 55, 1–30.
Schauer, U., 1995. The release of brine-enriched shelf water from the Storfjord into the Norwegian Sea. J. Geophys. Res. 100, 16015–16028.
Schauer, U., Fahrbach, E., 1999. A dense bottom water plume in the western Barents Sea: downstream modification and interannual variability. Deep-Sea Res. Part I 46, 2095–2108.
Skogseth, R., Fer, I., Haugan, P.M., 2005a. Dense-water production and overflow from an Arctic coastal polynya in Storfjorden. In: Drange, H., Dokken, T.,

Furevik, I., Gerdes, R., Berger, W. (Eds.), The Nordic Seas: An Integrated Perspective, Geophysical Monograph Series, vol. 158. AGU, Washington, DC, pp. 73–88.
Skogseth, R., Haugan, P.M., Jakobsson, M., 2005b. Watermass transformations in Storfjorden. Cont. Shelf Res. 25, 667–695.
Skogseth, R., Sandvik, A.D., Asplin, L., 2007. Wind and tidal forcing on the mesoscale circulation in Storfjorden, Svalbard. Cont. Shelf Res. 27, 208–227.
Skogseth, R., Smedsrud, L.H., Nilsen, F., Fer, I., 2008. Observations of hydrography and downflow of brine-enriched shelf water in the Storfjorden polynya, Svalbard. J. Geophys. Res. 113, C08049 10.1029/2007JC004452.
Uppala, S., Dee, D., Kobayashi, S., Berrisford, P., Simmons, A., 2008. Towards a climate data assimilation system: status update of ERA-Interim. ECMWF Newsletter 115. European Centre for Medium-Range Weather Forecasts, England, pp. 12–18.